JOURNAL OF MATERIALS SCIENCE 23 (1988) 769–775

Nitriding in the high temperature oxidation of Fe–31Mn–9Al–6Cr alloy

C. J. WANG, J. G. DUH*
Department of Materials Science and Engineering, National Tsing Hua University, Hsinchu, Taiwan, R.O.C.

An alloy, of Fe–31.3Mn–8.92Al–5.96Cr–0.86C composition, was heated from 800 to 1000° C in atmospheres of oxygen, nitrogen and dry air respectively. A needle-like structure was observed between the alloy matrix and the external oxidation layer in the nitrogen-containing atmosphere at temperatures higher than 800° C. The needle-like phase was identified as AlN by both X-ray and STEM diffraction methods. Nitriding first occurred in the austenitic grains adjacent to the free surface, with subsequent AlN growth towards the alloy matrix. The ferrite phase, formed due to the precipitation of chromium carbide, prevented the growth of AlN. For the alloy oxidized in air, AlN formed and the growth front of AlN was ahead of the oxides. The aluminium content of the alloy matrix in the nitrided region was depleted by the formation of AlN. Due to the rapid nitriding of Al, the formation of a protective oxide layer was retarded and the oxidation resistance became less promising.

1. Introduction

The Fe–Mn–Al based alloy system has attracted significant attention due to its potential as a substitute for conventional Fe–Ni–Cr stainless steel. The Fe–Al alloy is well known to have excellent high temperature oxidation resistance because of the formation of the protective α–Al_2O_3 layer during the oxidation process. This alloy is, however, brittle and has poor high-temperature strength due to its ferritic microstructure [1, 2]. The Mn–C combination, on the other hand, is believed to extend and to stabilize the austenite region in alloy steels which may have good high-temperature mechanical properties. Hence, an appropriate Fe–Mn–Al–C composition would possess good high temperature strength, low temperature workability, and better corrosion resistance [3–6].

Manganese and carbon in the Fe–Mn–Al–C system are elements which stabilize the austenite phase but are found to be detrimental to the high temperature oxidation resistance [7–9]. According to previous oxidation studies, an α–Al_2O_3 layer was frequently not observed in the austenitic Fe–Mn–Al–C alloys [10], or only discontinuous Al_2O_3 was found [9, 11]. It is argued that the presence of chromium leads to the formation of an α–Al_2O_3 by action as an oxygen getter [12, 13] or as a stabilizer of α–Al_2O_3 rather than the less protective γ–Al_2O_3 [2]. Hence, it is potentially promising to add chromium to the Fe–Mn–Al or Fe–Mn–Al–C alloys to improve the high temperature oxidation resistance [9, 14, 15].

During oxidation in dry air, it was observed that an Al-rich needle-like structure was formed beneath the oxide scale of Fe–Mn–Al alloys [11, 16, 17]. In the presence of the needle-like structure, the oxidation resistance of the alloy was poor. The needle-like structure was first considered to be an internal oxidation of aluminium [11]. Recently Lopes and Assuncao [18] indicated that it arose through nitriding of aluminium. Hence, this study investigates further the microstructure and morphological development of the needle-like structure. The role of the needle-like structure in the oxidation behaviour of the Fe–Mn–Al based alloy is revealed with the aid of electron microscopy and kinetic studies.

2. Experimental details

The chemical composition of the alloy employed in this study was Fe–31.30 wt% Mn–8.92 wt% Al–5.96 wt% Cr–0.86 wt% C. The alloy was prepared from high purity materials and melted in an argon shielded induction furnace. The ingot was forged to 75% reduction in thickness at 1200° C and then homogenized at 1200° C for 11 h. After surface finishing, the alloy was hot rolled at 1000° C to 90% reduction, giving a 2.5 mm thickness. In order to eliminate grain growth during oxidation and nitriding experiments, the hot rolled alloy was surface finished again and then annealed at 1150° C for 50 h in a tube furnace with flowing argon. Austenite was the only phase present in the specimen after annealing and the lattice parameter was determined to be 0.369 nm by X-ray diffraction.

The alloy was ground, and two kinds of specimens were prepared: one specimen, of dimensions 2 × 4 × 8 mm, was used for thermogravimetric analysis and for a morphological study; the other, of dimensions 2 × 10 × 20 mm, was employed for X-ray

*Will be on leave to the Department of Materials Science and Engineering, Cornell University, as visiting scientist, after 1 October 1987.

0022–2461/88 $03.00 + .12 © *1988 Chapman and Hall Ltd.*

analysis. All samples were abraded and polished with up to 0.05 μm alumina powder, ultrasonically washed in distilled water and rinsed in alcohol prior to oxidation and nitriding.

Experiments in this study were divided into three categories with respect to the atmosphere employed: (a) oxidation in pure oxygen; (b) oxidation in dry air; (c) nitriding in pure nitrogen. The gas flow was 200 c.c min^{-1} for each case. The temperatures for experiment in various atmospheres were set between 800 and 1000° C, and the time ranged from 2 to 48 h. Oxidation kinetics were recorded continuously for 24 h with a ULVAC/SINKU RIKO TGD–5000 thermogravimetric analyser. Specimens for morphological study and phase identification were either oxidized or nitrided in a horizontal tube furnace. Occasionally, the oxide scale spalled during cooling through the 300 ~ 350° C range. However, a technique was developed in this study to assure the integrity of the oxide layer. After oxidation, the test sample was dipped into 2 cm^3 of liquid zinc at 500° C, and then air cooled. The solidified zinc bar was successively cooled by a water quench. The total process took about 2 min and the alloy matrix/oxide scale was completely held by the presence of the solidified zinc.

Possible phases present in the specimen were identified with a Shimatzu X-ray diffractometer equipped with a Cu target, a Ni filter and a graphite single crystal monochrometer. Minor phases, of small size, were further identified by scanning transmission electron microscopy (STEM). Specimens for STEM studies were prepared with an ion mill (ION TECH B306 Super Microlap MK 2). The morphology of the oxide was examined with both the optical microscope (O.M.) and with the scanning electron microscope (SEM). Elemental distributions in the product layer were detected by X-ray mapping techniques and the characteristic nitrogen X-ray was measured with the STE analysing crystal with a computerized electron microprobe (JEOL JCXA–733). The nitride was qualitatively analysed with the energy dispersive spectrometer (EDAX 9100/70). In addition, quantitative analysis of the concentration of Fe, Mn, Al and Cr was performed with the aid of a ZAF-corrected program.

3. Results

3.1. Scale morphology in different atmospheres

The typical morphology of the alloy after oxidation at 1000° C in different atmospheres is shown in Fig. 1. Two oxide layers are observed in Fig. 1(a) for the alloy oxidized in oxygen. Fig. 1(b) presents the morphology of the alloy after nitriding in nitrogen; a region containing nitride is found beneath the free surface. The morphology of the alloy oxidized in air is shown in Fig. 1(c), which is apparently different from the oxidation morphology revealed in Fig. 1(a). The morphology of Fig. 1(c) is a mixture of the phases present in Figs 1(a) and 1(b).

For the specimens oxidized in pure oxygen in the temperature range 800 to 1000° C, $(Fe, Mn)_3O_4$ was present in the outer layer, and MnO, $MnAl_2O_4$, $Fe(Al, Cr)_2O_4$ and α–Al_2O_3 were revealed in the inner layer. A gap between the oxide layers was introduced during cooling which might be filled with the cold mount materials. A similar morphology was found at temperatures down to 800° C. Nevertheless, α–Fe_2O_3 and Mn_2O_3 were detected in the external oxide layer, and more chromium carbide and α grains were observed in the alloy matrix for those samples subjected to low temperature oxidation.

Referring to Fig. 1(c), it appears that three distinct products exist: the outer white region, the middle dark region and the inner grey region. Voids were believed to be formed during sample preparation, e.g. in polishing and etching. Phases in the outer layer are identified as $(Fe, Mn)_3O_4$. The inner grey layer is

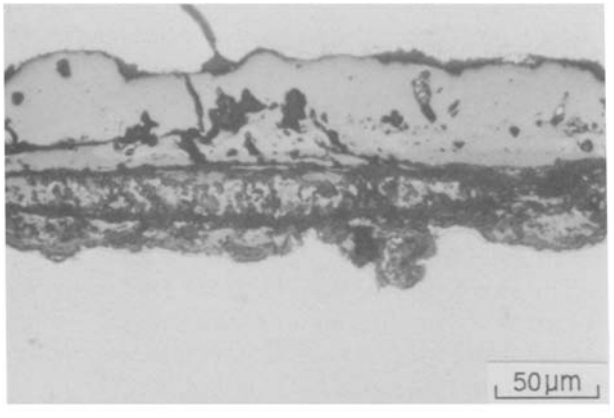

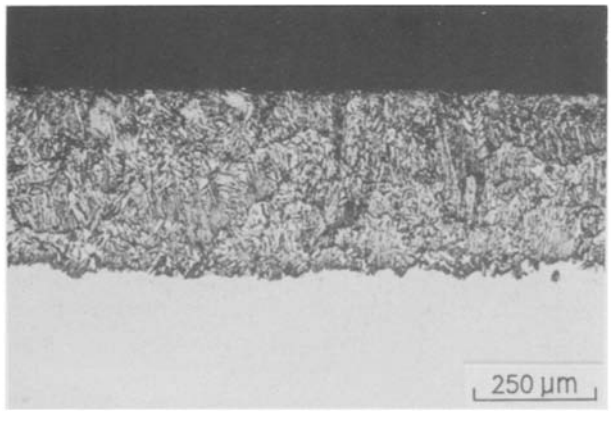

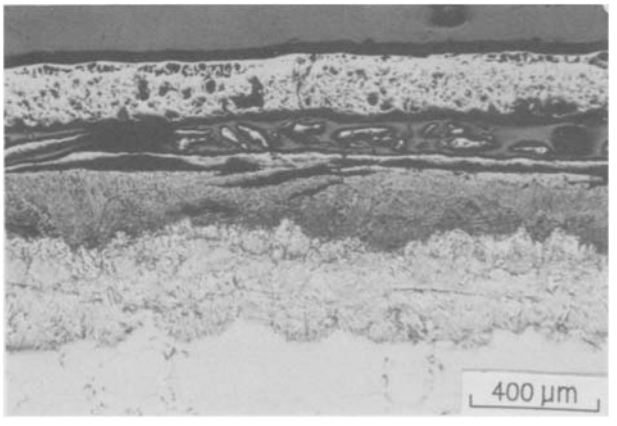

Figure 1 Optical micrograph of the specimen (a) oxidized in oxygen at 1000° C for 24 h (b) nitrided in nitrogen at 1000° C for 24 h (c) oxidized in dry air at 1000° C for 48 h.

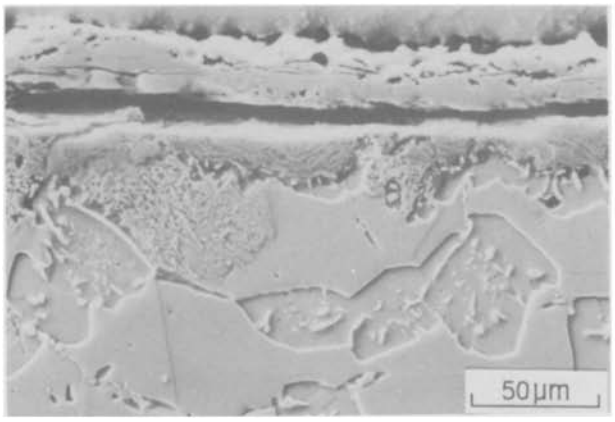

Figure 2 Scanning electron micrograph of the specimen oxidized in dry air at 850° C for 24 h, a region with the needle-like structure is visible beneath the oxide scale.

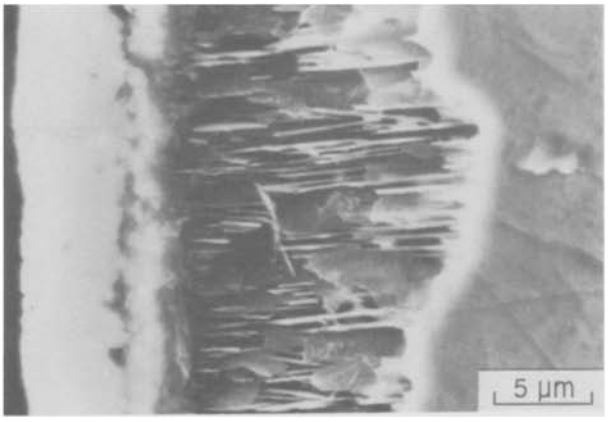

Figure 3 Scanning electron micrograph of the specimen oxidized in dry air at 1000° C for 10 min; an internal layer is evident as the needle-like structure.

similar to the nitrided region shown in Fig. 1(b). The needle-like structure as well as fine oxides are observed in the middle dark region. The oxides in the needles are MnO, and $Fe(Al, Cr)_2O_4$. The sample morphology was found for oxidation above 800° C. Fig. 2 shows the scanning electron micrograph of alloy oxidized in air at 850° C, and a region with needle-like structure is observed. The higher the temperature the more developed the needle-like structure approaching the case shown in Fig. 1(c). It was found that the morphologies of both oxides and the needle-like structure could be obtained when the alloy was oxidized at 1000° C in dry air for only 10 min as shown in Fig. 3. In general, the thickness of the product layer became enlarged as the oxidation time increased.

The needle-like structure is rich in aluminium as shown in the X-ray map (Fig. 4), whilst the region between the needle-like structure is aluminium-depleted. The composition of the region between the needle-like structure, e.g. the aluminium depleted region revealed in Fig. 4, was 66.05 wt % Fe, 25.95 wt % Mn, 7.02 wt % Cr and 0.08 wt % Al. The composition was quantitatively determined using an electron microprobe with the aid of pure element standards.

For the preliminary kinetic study, the specimen was introduced in the thermogravimetric analyser for the weight gain measurements. Fig. 5 presents the results for those alloys oxidized in both oxygen and dry air at 1000° C. It appears that specimens oxidized in dry air with the presence of the needle-like structure always have more weight gain than those oxidized in oxygen.

3.2. Phase identification in the needle-like structure

In order to identify the needle-like structure formed in dry air, an X-ray diffraction study was employed, using successively abraded samples. The X-ray diffraction pattern corresponding to the inner grey layer in Fig. 1(c) is represented in Fig. 6. The lattice parameter of the γ matrix, calculated on the basis of Fig. 6 was 0.364 nm, which was slightly smaller than that of the solution treated state. Although AlN appears to be identified in the diffraction pattern, the peak positions overlap with those of other oxides, such as $(Fe, Cr)_2O_4$, $\alpha-Al_2O_3$, $FeAl_2O_4$, and the γ matrix. Intensity ratios of the AlN found in this study did not, however, match exactly with the data in the literature [19]. As a consequence more analytical characterization is required to confirm the existence of the AlN structure. Fig. 7 shows the qualitative analysis of the needle-like structure by EDX. Similar to Fig. 4, it is apparent that Al is enriched in this structure. Nevertheless, whether it is an oxide or a nitride is unclear. The presence of nitrogen or oxygen characteristic X-rays can be further detected with an electron microprobe

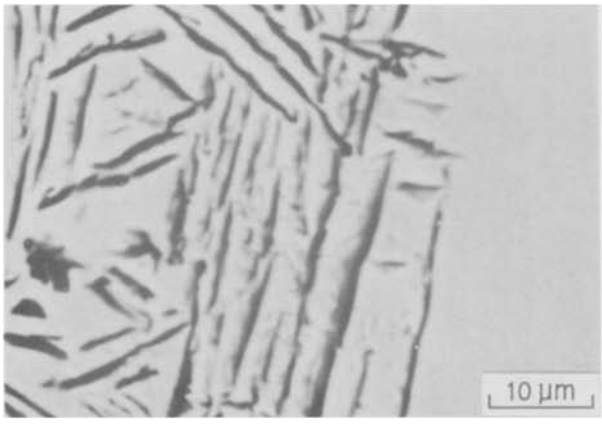

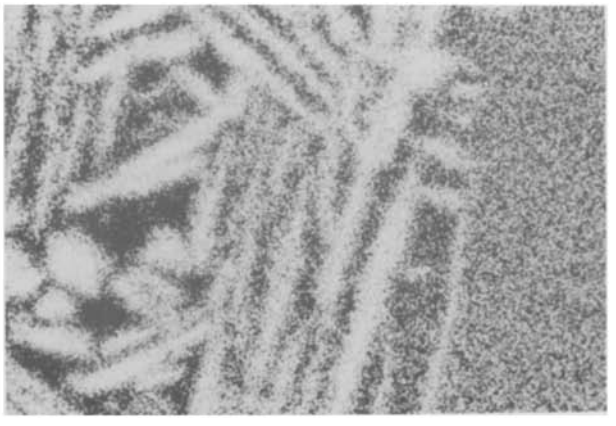

Figure 4 Scanning electron micrograph and X-ray images around the growth front of the needle-like structure as the specimen oxidized in dry air at 1000° C for 48 h: (a) SEM (b) Al Kα. (not etched).

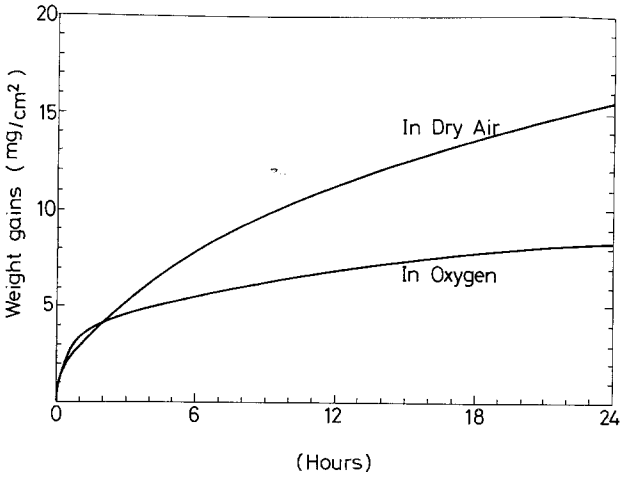

Figure 5 Continuous weight-gain curves for the specimen oxidized at 1000° C in dry air and in oxygen.

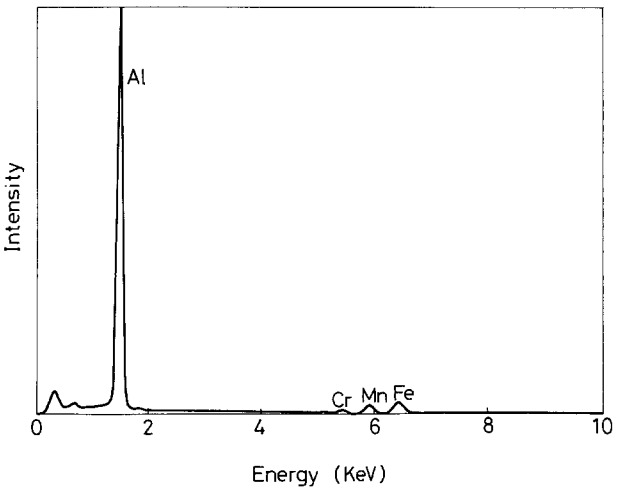

Figure 7 Qualitative analysis of the needle-like structure by EDX.

by employing the spectrometer step scanning technique. The variation of counts with spectrometer position is represented in Fig. 8. The peak position, 88130 μm, as read from Fig. 8 coincides with the theoretically calculated value for nitrogen $K\alpha_1$. Step scanning of the region near the expected value of oxygen was also made, but no peak was observed.

Selected area diffraction patterns (SADP) obtained from the inner grey layer in Fig. 1(c) are presented in Fig. 9. The sectioned plane in this study was parallel to the free surface of the specimen. The lattice parameter of the γ matrix, calculated from the SADP of Fig. 9(a), is 0.364 nm, which is compatible with the value from the X-ray diffraction pattern of Fig. 6. The SADP in Figs. 9(b–d) indicate that the needle-like structure is H.C.P. crystal structure with a = 0.311 nm and c = 0.495 nm. In agreement with previous studies [19, 20], the needle-like structure is identified as AlN. The corresponding STEM images are shown in Fig. 10.

3.3. Growth of AlN in nitrogen

Nitriding occurred when the temperature was greater than 800° C, and the width of the nitride region increased as the temperature was raised. It was observed that AlN was the primary product of nitriding as seen from Fig. 1(b). Based on Fig. 11, it is apparent that the shape of the needle-like structure is not related with the free surface. At lower temperature, a non-uniform nitride layer was observed as shown in Fig. 12. If the chromium carbide formed and ferrite precipitated, the growth of AlN detoured, as indicated in Fig. 12. Because of the orientation relationship, as indicated in Fig. 11, the grain boundary acts as the barrier for the growth of AlN. Fig. 13 presents the optical metallographic picture of the nitride-matrix interfacial region. It is observed that the growth of AlN tends to decelerate when approaching the grain boundary of the underlying matrix.

4. Discussion

Based on the results of qualitative elemental analysis and electron diffraction patterns, AlN is identified as the needle-like phase. The standard free energy of formation for AlN at 800 and 1000° C is −48.54 and −43.02 Kcal mole^{-1} respectively [21], which indicates the thermodynamic possibility of the formation of AlN within the temperature range of the present

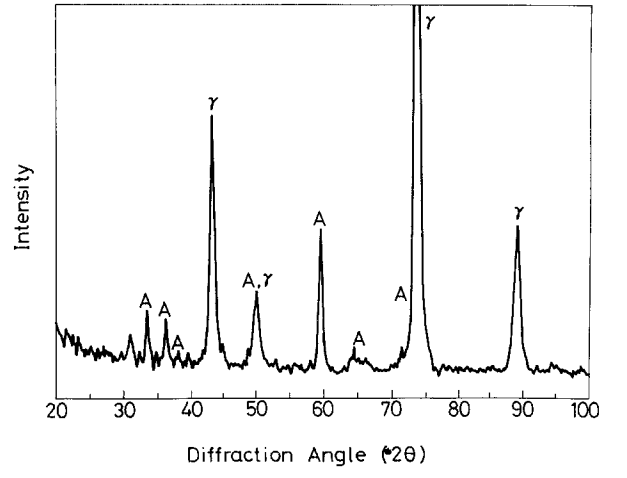

Figure 6 X-ray diffraction pattern of the specimen oxidized at 1000° C in dry air for 24 h; the specimen was abraded and the detected layer corresponded to the inner product layer in Fig. 1(c). (A : AlN, γ : Austenite).

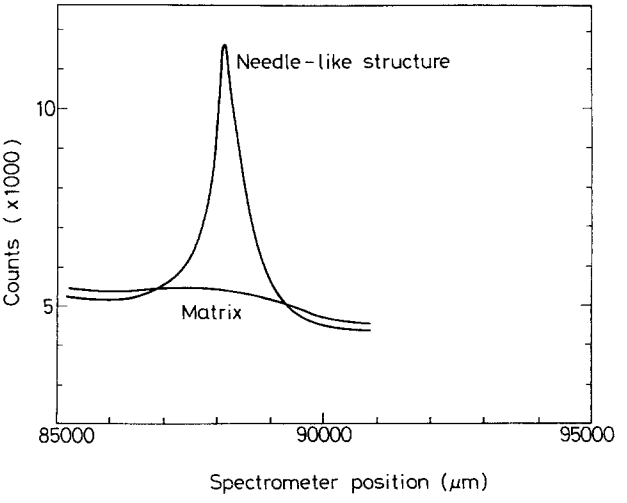

Figure 8 Intensity profiles of the matrix and the needle-like structure based on spectrometer step scanning.

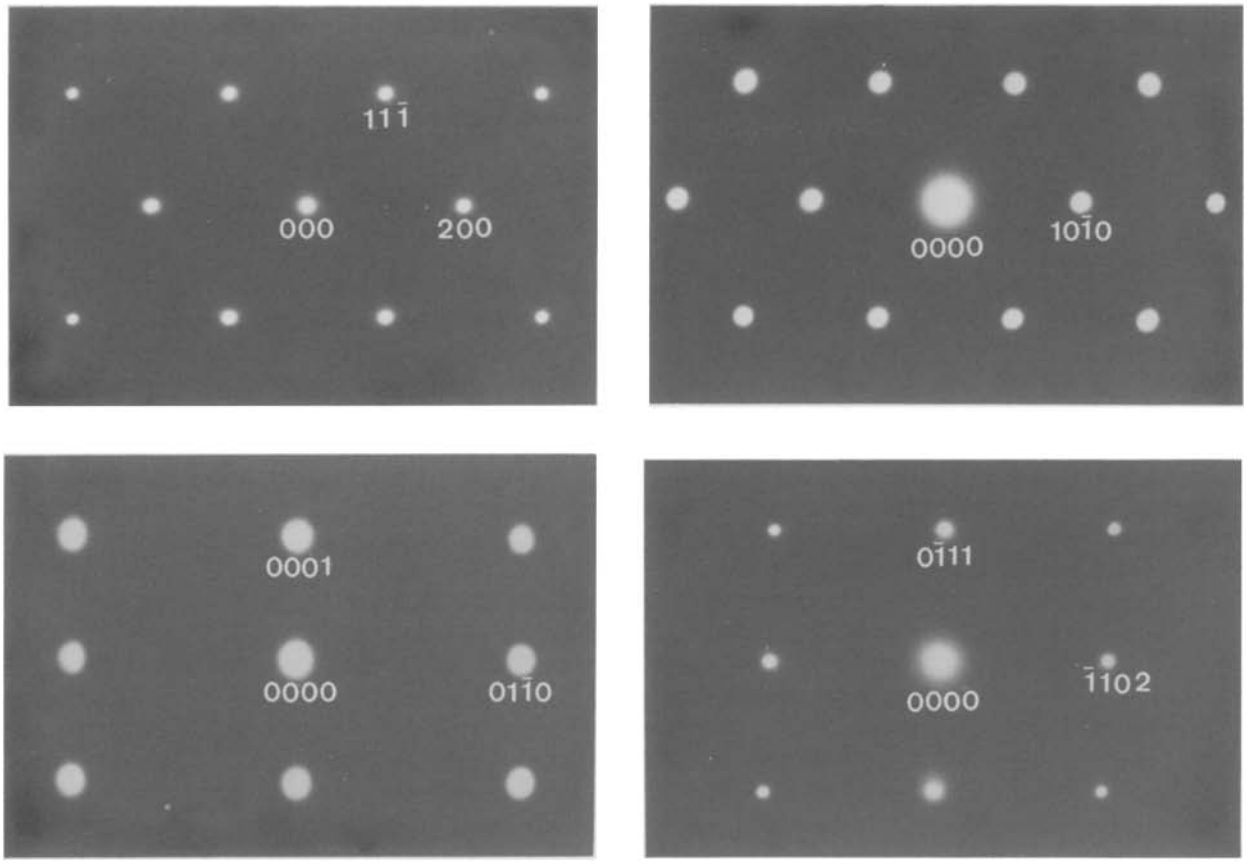

Figure 9 SAD patterns taken from the inner product layer in Fig. 1(c): (a) for the γ matrix, B = (0 1 1) (b) for AlN, B = (0 0 0 1) (c) for AlN, B = (2 1 1 0) (d) for AlN, B = (5 1 4 3).

study. It is reported that the solubility of nitrogen in the γ phase is greater than that in the α phase [22]. As shown in Fig. 12, AlN is observed only in γ grains although the α phase in this alloy has a greater aluminium content. This suggests that the γ phase, of higher nitrogen solubility, provides the easy path for nitrogen diffusion toward the alloy matrix and the presence of α or γ plays a major role in nitriding.

The structure of the alloy after annealing is fully austenitic before the oxidation and nitriding experiments. During oxidation, the formation of an α phase results from the precipitation of chromium carbide. At lower temperature, e.g. 850° C, the formation of carbide is favoured. The ferrite is formed by carbon depletion and results in a non-uniform nitride region as shown in Figs 2 and 12. As the temperature increases, the solubility of chromium and carbon in the Fe–Mn base alloy is increased. Nitriding is enhanced by the dissolved Mn and Cr in the austenite [23]. Hence, as the temperature increases, the thickness of the nitrided region increases since the reaction is promoted.

For experiments conducted in air, which contains both nitrogen and oxygen, nitriding and oxidation occur simultaneously. It is argued that nitrogen with an atomic radius of only 0.069 nm [24] might penetrate the oxide layer to react with the alloy matrix. In a study of oxidation in air of a Co–Cr–Al alloy by Giggins [25] and for pure Cr by Pettit [26], it was reported that nitride formed beneath the oxide layer. In the present study, it was observed that the nitride could be formed within a few minutes and grew ahead

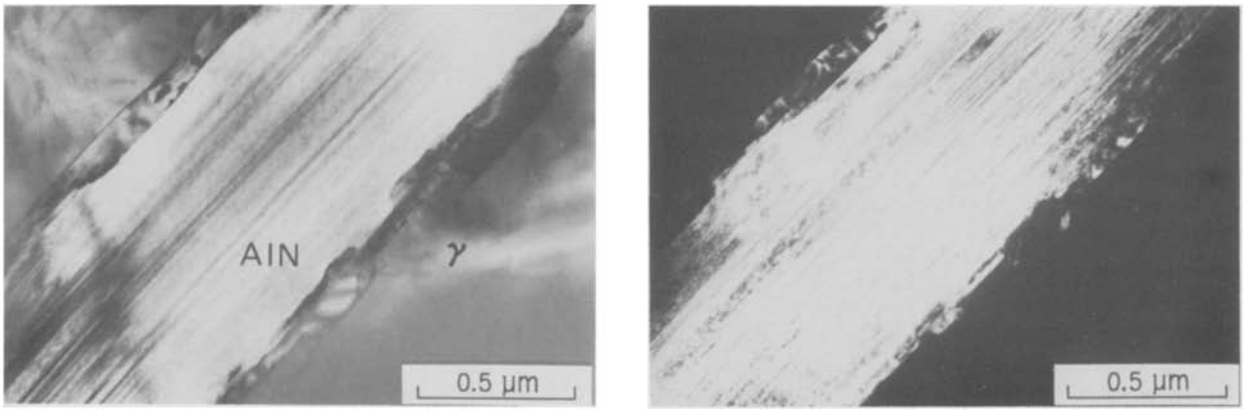

Figure 10 STEM microstructure of the inner product layer in Fig. 1(c): (a) bright-field image (b) dark-field image of AlN.

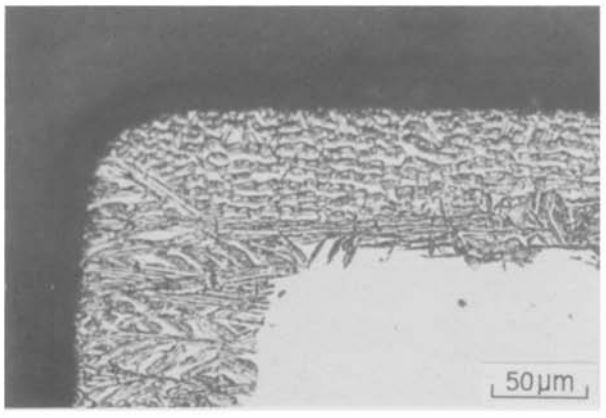

Figure 11 Optical micrograph of the specimen nitrided in nitrogen at 1000° C for 2 h.

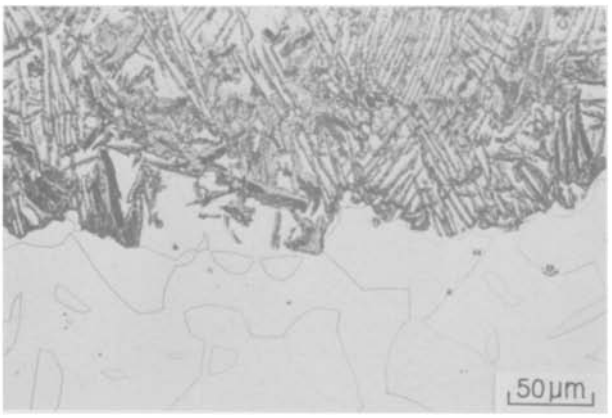

Figure 13 Optical micrograph of the interfacial region of AlN and γ matrix for the specimen nitrided in nitrogen at 1000° C for 24 h.

of the oxide layer as shown in Figs 1(c) and 3. As nitriding occurs prior to the oxidation and results in the needle-like AlN, the content of aluminium is depleted in this nitrided region and oxidation is dominated by Fe and Mn. Subsequently Fe and Mn diffuse out to form the $(Fe, Mn)_3O_4$ oxide. As a result, the oxide with the lower dissociation pressure, such as MnO, builds up by oxygen diffusing through the external oxide layer.

Thermodynamically, the free energy of α–Al_2O_3 is much lower than that of AlN, and AlN can be transformed as α–Al_2O_3 if the oxygen partial pressure is sufficient. This reaction could take place at the surface of AlN and result in a protective α–Al_2O_3 film [20]. As the AlN is shielded by the presence of α–Al_2O_3, the aluminium can not diffuse outwards to form the Al-rich oxides. In this study the Al-rich oxides, such as α–Al_2O_3 and $MnAl_2O_4$, are not observed, which is in agreement with the above statements. In short the needle-like AlN/γ interface would provide the easy diffusion path for oxidants including Fe, Mn, Cr and O. Hence this alloy has a higher oxidation weight gain compared with that oxidized in oxygen as shown in Fig. 5.

The effects of chromium in this alloy are considered with respect to the temperature employed. At low temperature, chromium enhances α precipitation by forming chromium carbide and prevents the infringement of nitrogen. At higher temperatures, more chromium is dissolved in the γ phase which acts as a binder for carbon [27]. In addition, it forms more Cr-containing oxide and thus retards the depletion of C and Mn during oxidation. As the γ phase prevails, the nitriding is promoted. This explains the phenomena observed in this study.

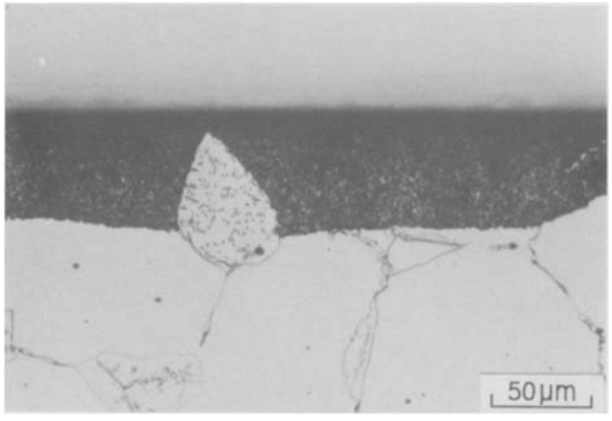

Figure 12 Optical micrograph of the specimen nitrided in nitrogen at 850° C for 2 h; ferrite is formed due to the precipitation of chromium carbide.

5. Conclusions

1. The Fe–31.30Mn–8.92Al–5.96Cr–0.86C alloy, heated in a nitrogen-containing atmosphere at temperatures greater than 800° C, developes a needle-like nitriding product of AlN which grows towards the alloy matrix. As the temperature is increased, the nitriding is enhanced.

2. For the alloy oxidized in air AlN also formed, and the growth front of AlN was ahead of the oxides. The needle-like AlN/γ interface provided an easy diffusion path for oxidants. The oxidation behaviour was dominated by Fe and Mn, and Al-rich oxides were not found. As a result, the observed weight gain was greater than that oxidized in oxygen at the same temperature.

3. AlN possesses a preferred orientation with its own grain rather than with the free surface. It was observed that the growth of AlN tended to decelerate when approaching the grain boundary of the underlying matrix.

4. The degree of the solubility of nitrogen plays the major role in alloy nitriding. The austenite phase with higher nitrogen solubility was observed to promote the growth of AlN, while the ferrite possessed the reversed effect.

Acknowledgements

The authors thank the National Science Council, Taiwan, R.O.C. for the financial support under the contract No. NSC–76–0405–E007–11. The helpful discussions with Professor C. M. Wan are acknowledged.

References

1. W. E. BOGGS, *J. Electrochem. Soc.* **118** (1971) 906.
2. W. C. HAGEL, *Corrosion* **21** (1956) 316.
3. S. K. BANERJI, *Met. Prog.* **113** (1978) 79.
4. S. K. BANERJI, in Proceedings of the "Workshop on Conservation and Substitution Technology for Materials", Vanderbilt University, Nashville, Tennessee, USA, June (1981).

5. S. K. BANERJI, in "The Public Workshop on Trends in Critical Materials Requirements for Steels of the Future–Conservation and Substitution Technology for Chromium", Vanderbilt University, Nashville, Tennessee, USA, October (1982).
6. R. WANG and F. H. BECK, *Met. Prog.* **123** (1983) 72.
7. C. H. KAO, C. M. WAN and M. T. JAHN, in "Alternate Alloying for Environmental Resistance", edited by G. R. Smolik and S. K. Banerji (The Metallurgical Society, Inc., 1987) p. 299.
8. C. H. KAO and C. M. WAN, *ibid,* p. 355.
9. P. R. S. JACKSON and G. R. WALLWORK, *Oxid. Met.* **21** (1984) 135.
10. C. H. KAO, C. M. WAN and M. T. JAHN, in "Alternate Alloying for Environmental Resistance", edited by G. R. Smolik and S. K. Banerji (The Metallurgical Society, Inc., 1987) p. 347.
11. J. P. SAUER, R. A. RAPP and J. P. HIRTH, *Oxid. Met.* **18** (1982) 285.
12. P. TOMASZEWICZ and G. R. WALLWORK, *Oxid. Met.* **20** (1983) 75.
13. C. WAGNER, *Corr. Sci.* **5** (1965) 751.
14. J. G. DUH, C. J. LIN, J. W. LEE and C. M. WAN, in "Alternate Alloying for Environmental Resistance", edited by G. R. Smolik and S. K. Banerji (The Metallurgical Society, Inc., 1987) p. 283.
15. S. C. CHANG, S. C. CHEN and J. F. LIU, in Proceedings of the 4th Asian–Pacific Corrosion Control Conference, Tokyo, Japan (May 1985) p. 47.
16. C. J. WANG, MSc thesis, National Tsing Hua University, Taiwan, R.O.C. (1984).
17. J. G. DUH, C. J. WANG, C. M. WAN and B. S. CHIOU, in "Alternate Alloying for Environmental Resistance", edited by G. R. Smolik and S. K. Banerji (The Metallurgical Society, Inc., 1987) p. 291.
18. M. F. SILVA LOPES and F. C. RIZZO ASSUNCAO, *ibid,* p. 321.
19. NBS Monograph 25, Sec. 12 (1974).
20. K. M. TAYLOR and C. LENIE, *J. Electrochem. Soc.* **107** (1960) 308.
21. D. R. STULL and H. PROPHET, JANAF Thermochemical Tables, NSRDS–NBS37, U.S. Dept. Commer., Washington, D.C. (1971).
22. K. KIUCHI and R. B. McLELLAN, *Met. Trans.* **15A** (1984) 199.
23. ASM: Metals Handbook, 8th ed. Vol. 8, ASM (Metals Park, Ohio 1973) p. 412.
24. H. J. GOLDSCHMIDT, in "Interstitial Alloys", (Plenum, New York, 1967) p. 214.
25. G. S. GIGGINS and F. S. PETTIT, *Oxid. Met.* **14** (1980) 363.
26. F. S. PETTIT and G. W. GOWARD, in "Coatings for High Temperature Applications", edited by E. Lang (Applied Science Publishers, New York, 1983) p. 1.
27. A. U. MALIK, *Oxid. Met.* **25** (1985) 233.

Received 9 February 1987
and accepted 22 October 1987